Functionalization of Multiwalled Carbon Nanotubes by Mild Aqueous Sonication

De-Quan Yang, Jean-Francois Rochette, and Edward Sacher*

Regroupement Québécois de Matériaux de Pointe, Département de Génie Physique, École Polytechnique, C.P. 6079, succursale Centre-Ville, Montréal, Québec H3C 3A7, Canada

Received: October 25, 2004; In Final Form: January 27, 2005

Sonication has been widely used in the dispersal of carbon nanotubes (CNTs) in various liquids as well as in their functionalization in aqueous acids. Here, for the first time, we study the sonication of multiwalled CNTs (MWCNTs) in deionized water. Our results indicate an improvement in the aqueous dispersal of MWCNTs as well as an increase in their adhesive interaction with Au substrates. Field emission scanning electron and high-resolution transmission electron microscopies as well as X-ray photoelectron, photoacoustic Fourier transform IR, and Raman spectroscopies have shown this to be due to the production of low concentrations of O-containing functionalizations (alcohol, carbonyl, acid, with the total O concentration being ∼2%), without damaging the basic CNT structure; this production of functional groups is mirrored by the disappearance of $-CH_n$ groups existing on the pristine CNTs. These new functional groups are capable of hydrogen bonding, which plays an important role in their aqueous dispersal and enhanced substrate interactions.

Introduction

The separation and dispersal of carbon nanotubes (CNTs) has attracted much attention because they are difficult to disperse, due to interactions and entanglements. This has resulted in their poor processability for many potential applications. The main pathway toward dispersal has been via the production of surface modifications, which introduce lyophilic functional groups.[1−8] There are three methods that have been used to accomplish this: (1) chemical oxidation in aqueous media,[9] where the acid not only dissolves any remaining metal catalyst but it also removes the CNT end cap, leaving carboxylic acid (−COOH) residues that are not only hydrophilic but, in basic solution, where the groups exist as $-COO^-$, lead to CNT−CNT repulsion; (2) the adsorption of surfactants (e.g., sodium dodecyl sulfate (SDS) and Triton X-100)[10] and polymers[8] by the walls of the CNTs during sonication, where the dispersal efficiency appears to depend on the presence of hydrophilic groups;[11] (3) covalent interactions leading to the attachment of hydrophilic groups.[2]

While much significant progress has been made in research on the dispersal of CNTs, it is obvious that extensive and severe chemical modification may strongly modify their electrical, mechanical, and optical properties that are so critical to their commercialization. An additional problem, in the case of CNT dispersal by surfactants, is the necessity for ultimate surfactant removal.

Sonication is used to accelerate the dispersal of CNTs by the techniques already mentioned. In these cases, sonication is used to introduce an energy density, at the CNT−CNT interface, sufficiently high to cause initial separation; this permits access to the CNT surface by the treatment chosen to maintain dispersal. The defect density produced on the CNT depends not only on the sonication power but, also, on the treatment medium.[12] Indeed, oversonication may lead to the formation of amorphous carbon particles, shortening the lengths of the CNTs, and conversion into rods.[12,13]

Here, for the first time, we explore the effect of sonication on MWCNTs in pure deionized water, the solvent generally used for CNT treatment. We observed a significant improvement in CNT dispersal on sonication in pure water. Chemical and physical changes were characterized by field emission scanning electron (FESEM) and high-resolution transmission electron (HRTEM) microscopies, X-ray photoelectron (XPS), photoacoustic Fourier transform IR (PAFTIR), and Raman spectroscopies. The results give an understanding of the sonication process and its effect on CNT dispersal.

Experimental Section

Multiwalled CNTs (MWCNTs, greater than 95% pure, diameter 10−20 nm, length 1−5 μm) were obtained from Nano-Lab, Brighton, MA (http://www.nano-lab.com/carbonnanotubes.html). The manufacturer indicates that the CNTs contain less than 5% impurities, including residual catalyst; this indicates that the amorphous content is substantially less that 5%, making contaminant detection by HRTEM problematic. Indeed, previous HRTEM[14,15] studies on the same CNTs used here did not detect amorphous material. Cyclic voltammetry on these same CNTs,[14,15] which requires conducting pathways, supports this absence of amorphous material. Our own HRTEM study on pristine and sonicated MWCNTs (see Supporting Information) shows that no amorphous contaminant is produced, even after extensive sonication.

Sonication was carried out in 18 MΩ water, at room temperature, using a Branson Bransonic 2200 ultrasonic cleaner, operating at 40 kHz. We found that the ease of dispersal increased with sonication time: while unsonicated CNTs could not be dispersed in deionized water, 2 min of sonication permitted some dispersal, and CNTs sonicated for 45 min formed a dispersion stable for at least 3 weeks.

The dispersed CNTs were dropped onto Au-coated (200 nm Au/10 nm Ti) Si wafer segments, 15 × 15 mm^2. They were then dried, at room temperature, under several Torr of mechan-

* To whom correspondence should be addressed. E-mail: edward.sacher@polymtl.ca. Tel: (514) 340-4711 ext. 4858. Fax: (514) 340-3218.

10.1021/jp045147h CCC: $30.25
Published on Web 03/24/2005

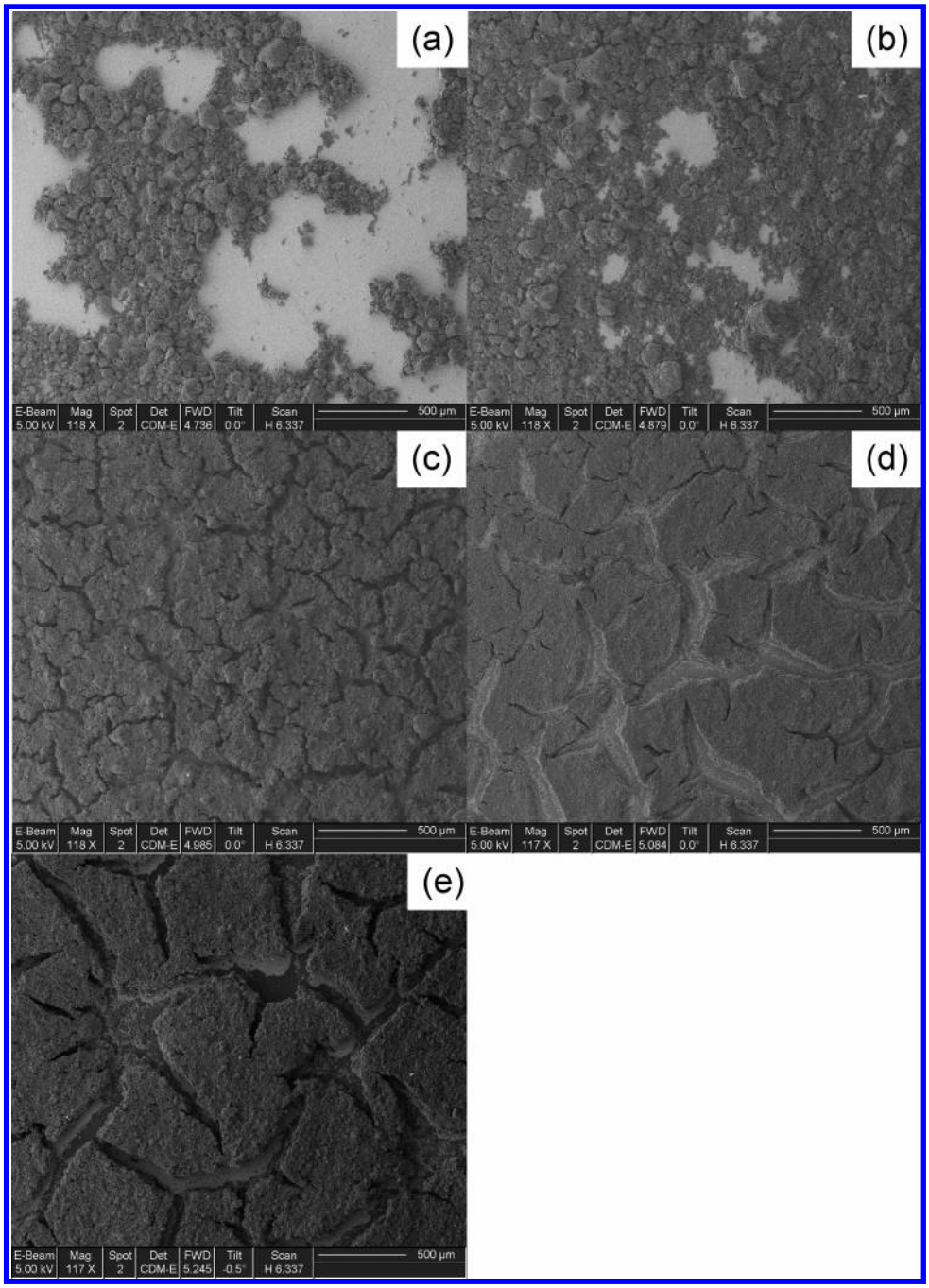

Figure 1. FESEM photomicrographs of MWCNTs on the Au surface, as a function of sonication time: (a) untreated, (b) 30 s, (c) 2 min, (d) 15 min, and (e) 45 min.

ical pump vacuum, for at least 24 h. FESEM photomicrographs were obtained on a FEI FBI-DB235 with the experimental parameters used appearing on the photomicrographs.

XPS was carried out in a VG ESCALAB 3 Mark II, using nonmonochromated Mg Kα X-rays (1253.6 eV), at a pressure of less than 10^{-10} Torr. High-resolution spectra were obtained at a perpendicular takeoff angle, using a pass energy of 20- and 0.05-eV steps. The spectral resolution was ~0.7 eV. After Shirley background removal, the component peaks were separated by the VG Avantage V 1.62 (Thermo VG Scientific) software.

Photoacoustic Fourier transform IR spectroscopy (PAFTIR) was carried out using a He-purged MTEC 300 photoacoustic cell in a Bio-Rad FTS 6000 spectrometer, at a spectral resolution of 4 cm^{-1}. The 5 kHz modulation frequency used probed the entire sample thickness. CNT samples for analysis were made by dropping and drying, using n-doped Si wafers with native oxide.

Results

FESEM Observations of Sonicated MWCNTs. Morphological changes on sonication, obtained by FESEM, are seen in Figure 1. Interaction between the CNTs and the substrate increased with sonication time; significant changes were seen for times as short as 2 min. The interaction was manifested as an increased wettability of the substrate surface; such interaction is stronger than CNT−CNT interactions, as manifested by cracks in the CNT layer, rather than a loss of CNT adhesion to the Au substrate.

The extent of CNT interaction with the Au substrate is seen by the fact that the adhesion between CNTs, deposited from a dispersion onto an Au substrate, increases with sonication time.

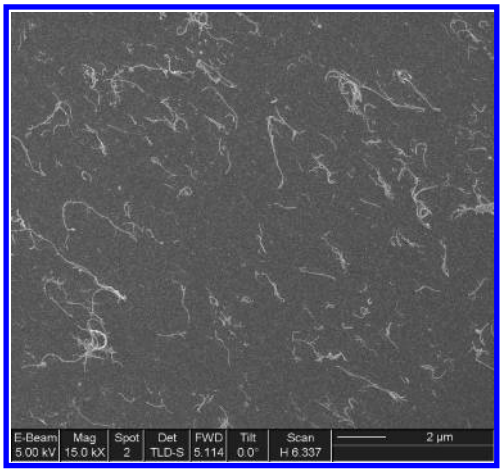

Figure 2. A FESEM photomicrograph of individual MWCNTs on a Au surface, deposited after 45 min of sonication. The sample was produced by diluting the sonicated solution before depositing, washing with water, and drying.

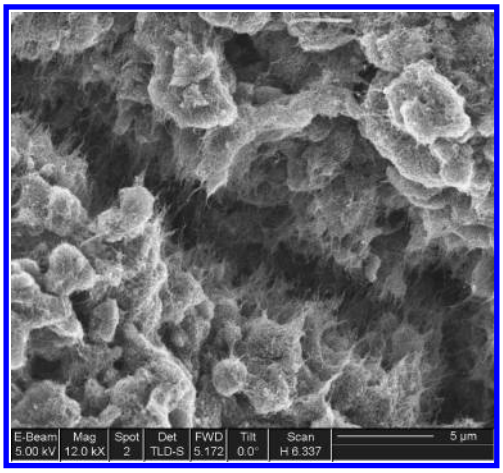

Figure 3. A FE SEM photomicrograph of the CNT alignment in the crack region of a MWCNT film deposited after 45 min of sonication.

While unsonicated CNTs can be washed off the Au substrate with running water, sonicated CNTs cannot. An example is seen in Figure 2, where a CNT sample, sonicated for 45 min, was intentionally diluted with water, immediately after sonication, before dropping onto the Au substrate to permit individual, well-separated CNTs to be seen. Once dried, such CNTs cannot be washed away in running water. All the CNTs in Figure 2 are seen to lie horizontally, in a random orientation; this was invariably found, strongly suggesting that CNT−substrate interactions occur along the length of the CNTs and not at their ends.

CNT−CNT interactions are seen in the CNT orientations evident in the crack regions, as found in Figure 3 for a sample subjected to 45 min of sonication. It is improbable that the clumps, also seen in Figure 3, exist prior to drying, since such clumps would not give the stable dispersion obtained after 45 of sonication, as mentioned earlier. Figure 1 shows much larger clumps present in the absence of sonication, and their size is reduced with sonication time; thus, while smaller clumps probably exist in the present dispersion prior to sample formation, they are too small to destabilize the dispersion; free CNTs appear to have aggregated around already existing microclumps while drying, during sample formation. This is another demonstration of CNT−CNT interactions. The sources of both CNT−substrate and CNT−CNT interactions will be discussed later, after the development of the chemical characterization data that reveal them.

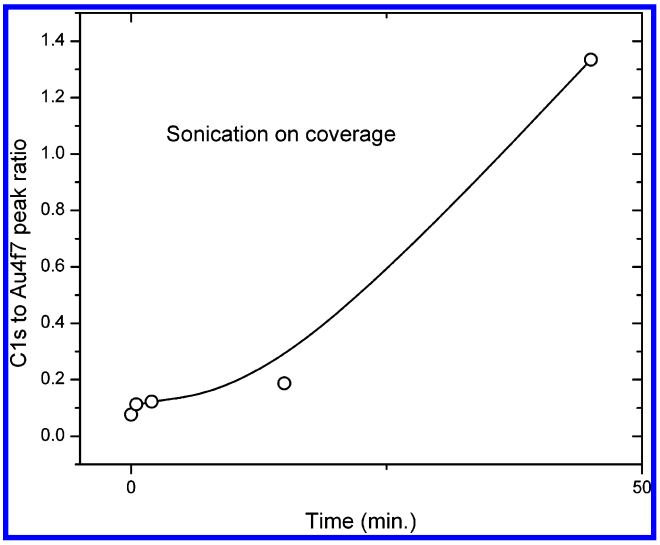

Figure 4. The ratio of XPS C1s to Au $4f_{7/2}$ peak areas, as a function of sonication time.

No shortening of the CNTs and no obvious damage were seen, even after 2 h of sonication, which is consistent with previous reports that an aqueous medium causes little damage[12] (see, also, Supporting Information).

XPS Analysis. XPS analysis indicated the expected presence of C, a trace amount of O, and Au due to the porosity of the CNT layer. The C1s:$Au4f_{7/2}$ peak area ratio, which is a measure of CNT coverage (the loss of porosity, as well as the appearance of cracks), is shown in Figure 4. The CNT coverage clearly increases with sonication time, consistent with the FESEM observations, above. That is, increased sonication increases CNT−Au substrate wettability.

The C1s spectrum, on sonication, is seen in Figure 5a, where it is compared with that of highly oriented pyrolytic graphite (HOPG); the shake-up region, near 291 eV, is enlarged in Figure 5b. The full width at half maximum (fwhm) of the main peak, in Figure 5a, was found to be 1.05 ± 0.05 eV for HOPG and 1.20 ± 0.05 eV for the CNTs with no change and within experimental error on sonication. This constitutes further evidence for the absence of amorphous material in the pristine CNTs: were amorphous material being produced on sonication, the fwhm would have broadened, as was found for HOPG[16], and had it been consumed, the fwhm would have narrowed. The response of the fwhm to the presence of amorphous material is sensitive to less than 0.1 monolayers.[14,18]

Because the fwhm of C1s is directly related to the electronic state of the CNTs, the wider fwhm for CNTs, as noted above, indicates a less delocalized electron density compared to HOPG, consistent with a greater presence of chemical groups in the MWCNTs, whose presence disrupts electron delocalization. Despite this, there was no noticeable change on sonication for either the main peak, in Figure 5a, or the shake up, in Figure 5b; the apparent height increase of the CNT shake up over that of HOPG is due to the overlap of the wider CNT main peak in Figure 5a. There was no noticeable change in the CNT spectra on sonication, suggesting that any change that occurred was too small to be seen over the existing spectrum. This indicates a low density of the previously mentioned chemical groups that disrupt electron delocalization.

In contrast to the unchanging C1s spectrum, the O1s spectrum in Figure 6 underwent noticeable changes, indicating that sonication affected the chemical structures of the O-containing

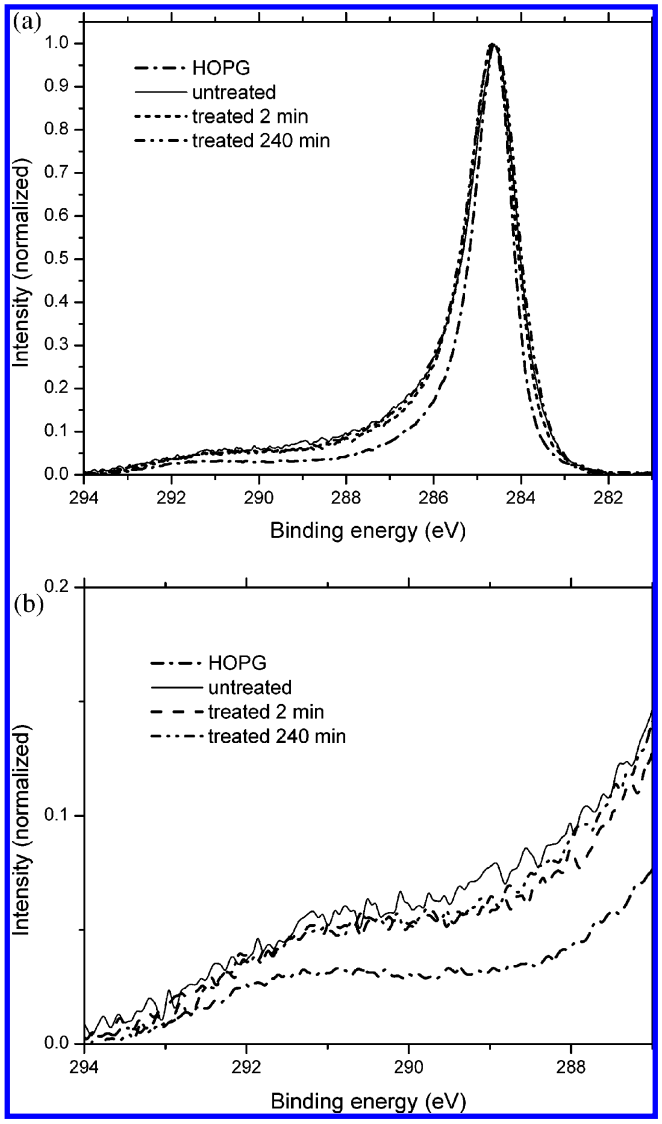

Figure 5. A comparison of C1s XPS (a) main peak and (b) shake-up spectra of MWCNTs as a function of sonication time.

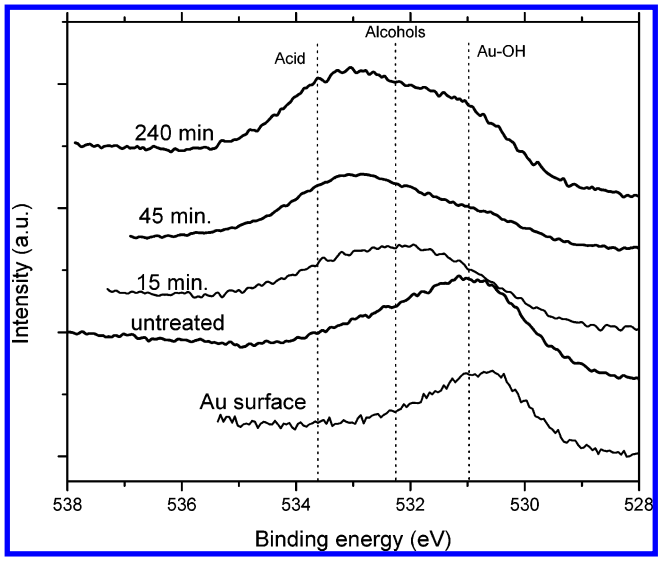

Figure 6. The evolution of the O1s XPS spectrum of MWCNTs, as a function of sonication time.

species. Peak separations used the components seen in Figure 7: the O1 component, at 531.0 ± 0.1 eV, has the same binding energy as the O1s peak from a bare Au surface and is attributed

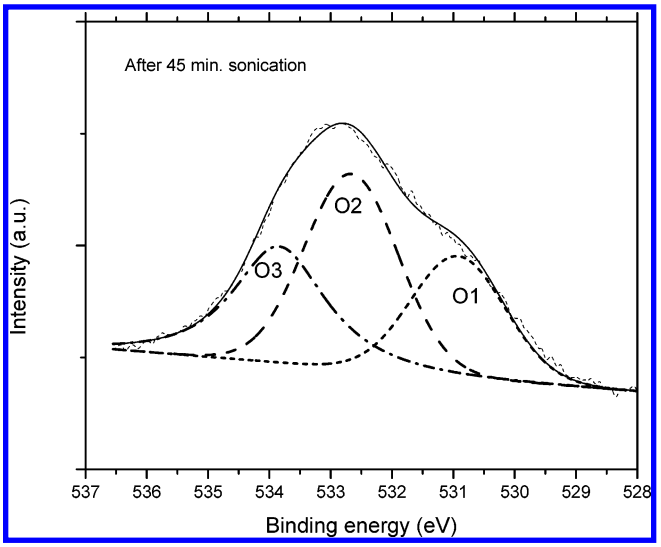

Figure 7. A typical O1s XPS spectral separation of MWCNTs (after 45 min of sonication).

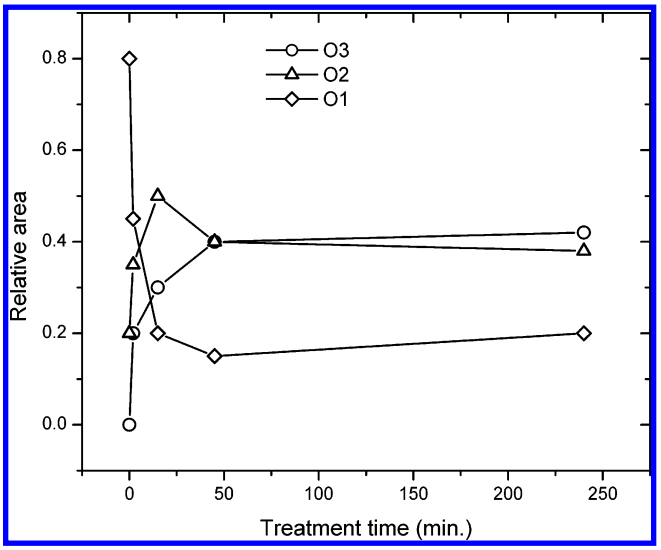

Figure 8. The evolution of O1s spectral components, as a function of sonication time.

to the oxidized Au surface, which reacts with humidity to form Au−OH.[16] The O2 component, at 532.7 ± 0.1 eV, is attributed to carbonyl (−C═O) and alcohol (−OH)[17] and the O3 component, at 534.2 ± 0.1 eV, to carboxylic acid (−COOH).[17] The O1s peak envelope shifted to higher binding energy upon sonication, indicating a continued increase, from lower to higher oxidation states, during sonication.

The relative peak areas, as a function of sonication time, are found in Figure 8 and the overall O concentration, in Figure 9. The O1 (substrate) component decreased rapidly on sonication, in Figure 8, as the O3 (acid) component increased; the O2 (carbonyl and alcohol) component increased initially, before decreasing slightly and stabilizing. Figure 9a shows that the overall O concentration, still below 3%, initially surged. As Figure 9b shows, this is due to the initial surge of the −OH and C═O formed (O2), followed by a less rapid increase as −COOH began to form (O3) from the −C═O present. This low concentration of O-containing species, on the CNT surface, is too small to be seen in the C1s spectrum of Figure 5.

Raman Spectra. The Raman spectra of the sonicated MWCNTs are found in Figure 10 and are compared to that of HOPG. A strong G band appears at ∼1572 cm^{-1} for the CNTs, slightly shifted from the G band of HOPG (1580 cm^{-1}). There is a

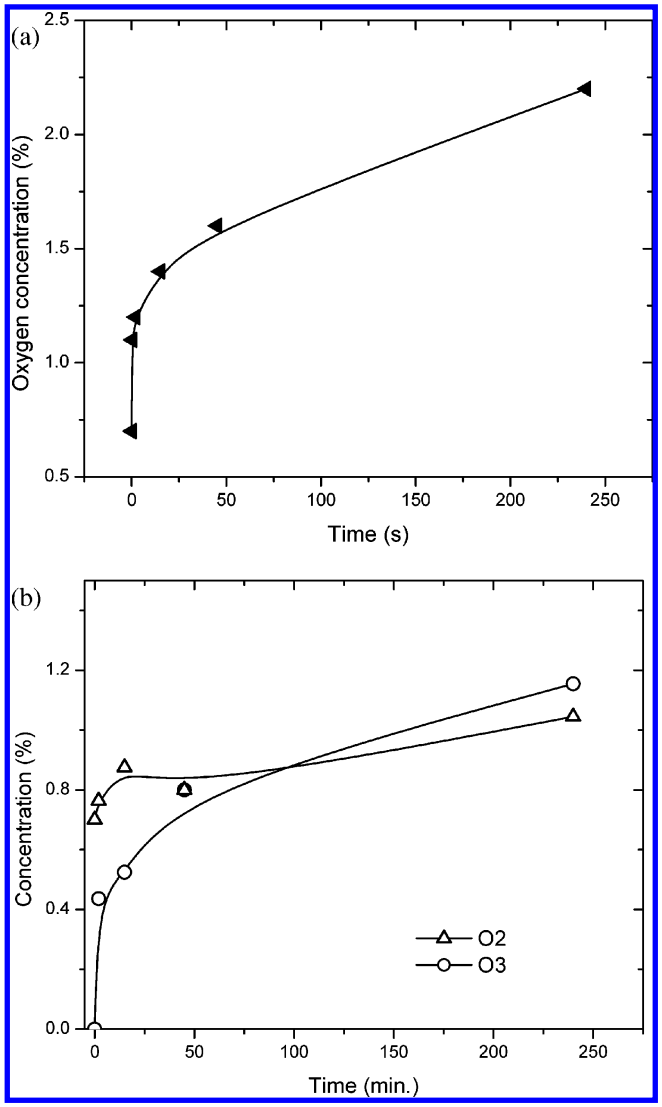

Figure 9. The XPS-determined relative oxygen concentration, as a function of sonication time: (a) total concentration (including oxygen from substrate); (b) oxygen from carbon nanotubes (O2 and O3).

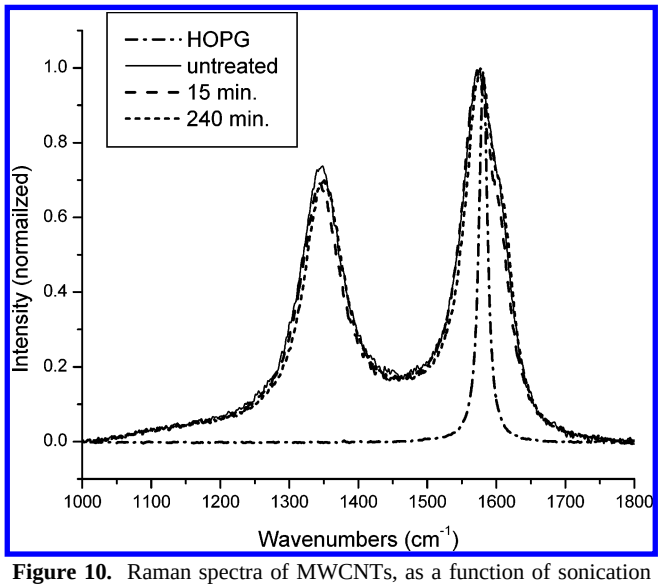

Figure 10. Raman spectra of MWCNTs, as a function of sonication time. The spectrum of HOPG is added for comparison.

noticeable shoulder on the CNT G band, ~1601 cm^{-1}. This shoulder was also found in our previous HOPG study after low-energy Ar^+ treatment;[18] it does not appear to be due to previously attributed finite size effects[19] but is, rather, defect related. A disorder-induced CNT D band appears at ~1345 cm^{-1}, attributable to lattice distortions, the presence of structural defects (such as unexpected chemical groups), or both. The present D band position is consistent with previously reported values.[18] There were no observable variations of either the G or D bands upon sonication, indicating that the changes introduced on sonication are neither new nor extensive and (2) again confirming the lack of amorphous material in the pristine CNTs.

TABLE 1: Attribution of Principal PAFTIR Peaks of the CNTs

peak (cm^{-1})	attribution	ref
~2890−2960	CH_n stretching	25
1680	CNT skeletal in-plane vibration	25
	C═O stretching	24, 25
1540	CNT skeletal in-plane vibration	25
1460	CNT skeletal in-plane vibration	25
	CH_n deformation	25

Photoacoustic FTIR. Despite the extensive use of Raman spectroscopy in the study of CNTs, there have been few investigations using FTIR.[20−24] The information obtainable has been limited and not well identified because of the presence of a strong CNT background absorbance.[21,22] While both transmission and reflectance FTIR produce weak spectra, PAFTIR offers more information because, as in this case, it may be used to obtain spectra from opaque samples. Table 1 indicates the attribution of principal PAFTIR peaks of the CNTs. Figure 11a show PAFTIR spectra of MWCNTs, as a function of sonication time, with the spectrum of HOPG shown for both comparison and peak attribution. While here, too, there is a strong background and the FTIR signal is difficult to see, the spectrum obtained is similar to those previously obtained in both transmission and reflection.[20−24]

Although the spectral slopes of HOPG and the untreated CNTs are similar, those for the CNTs increase with sonication time. To better see the IR signal, we have performed an arbitrary background subtraction, to give the spectra in Figure 11b for several sonication times; the spectrum of HOPG is also included. Several things are seen to occur on sonication. Among them, the initial presence of multiple $-CH_n$ stretching peaks across the 2880−2990-cm^{-1} range indicates the presence of $-CH_n$ species (i.e., −CH, $-CH_2$, and $-CH_3$).[25] The rapid disappearance of this multiplet, on sonication, mirrors the surge found for −OH and −C═O production in Figures 8 and 9.

Further, while the peaks in the range 1540−1680 cm^{-1} are known to have components due to CNTs skeletal motions,[23,24] they also have components due to O-containing moieties;[25] aromatic acids, aldehydes, and ketones all exhibit −C═O stretching peaks near 1680 cm^{-1}. Further, $-CH_n$ deformations occur near 1540 cm^{-1}. It is, then, interesting to note that, on sonication, the ratio of the 1650-:1540-cm^{-1} bands, a maximum for HOPG, decreases with sonication time; while the ratio may possibly reflect changes in the CNT structure (although such absorption bands are quite different from the ones found here[23,24]), it probably reflects the oxidation of $-CH_n$, confirming the XPS results.

Discussion

The MWCNTs used here are greater than 95% pure, containing some residual catalyst but little or no amorphous material. This was confirmed in prior HRTEM[14,15] and cyclic voltammetry[14,15] studies as well as in our present HTREM (see Supporting Information), XPS, and Raman results. Thus, the

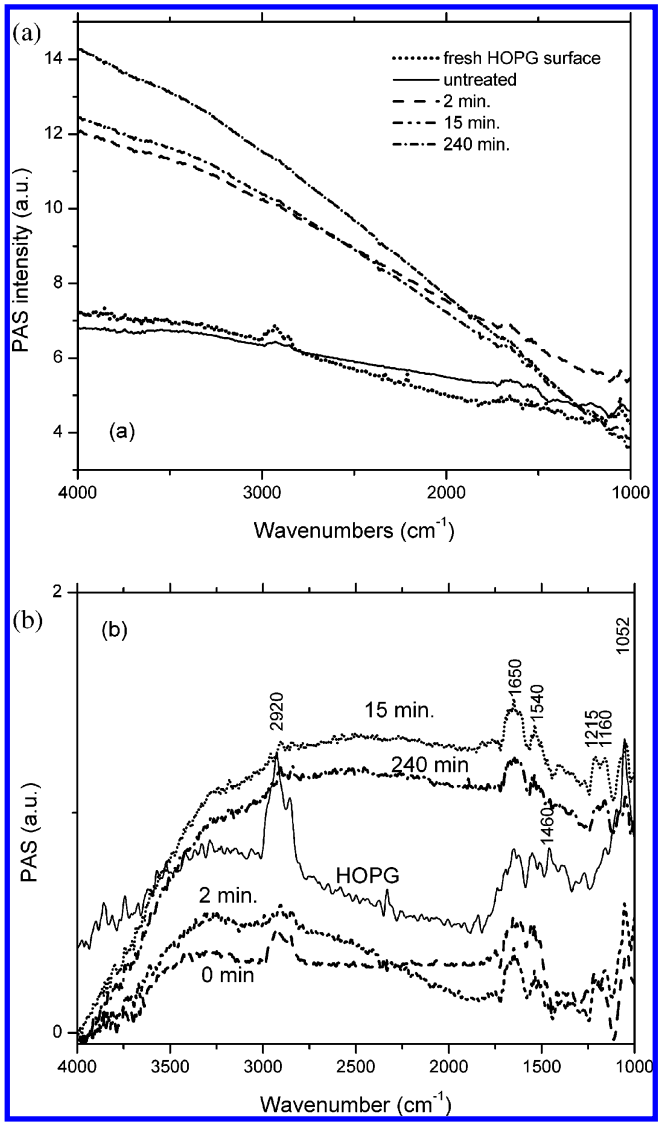

Figure 11. The evolution of the photoacoustic FTIR spectra of MWCNTs, as a function of sonication time: (a) as acquired and (b) after arbitrary background subtraction. The spectrum of HOPG is added for comparison.

defect chemical groups under discussion are present on the CNTs themselves.

The morphological evidence offered by our FESEM study indicates an increase in MWCNT interaction with the Au substrate on increasing the aqueous sonication time. This is due to the fact that such sonication can be used to affect chemical changes, under mild contentions, which may then be used for further reaction. These chemical changes occur along the lengths of the NTs, and not at their ends.

The XPS results, using fwhm measurements of the C1s spectrum[18,26] and peak attributions in the O1s spectrum, indicate the progressive oxidation of existing defect chemical groups (i.e., $-CH_n$) rather than their sonication-initiated introduction. Further, the C1s fwhm value, and its lack of change on sonication, indicate that detectable amorphous material is both initially absent and not formed on sonication, eliminating amorphous material as the oxidation site. This is confirmed by the Raman results, since the introduction of new defects would cause changes in the G and D bands;[18] such changes are absent here. PAFTIR spectral analysis indicates that these defect groups are $-CH_n$ and that they are oxidized by aqueous sonication.

The background slopes of the PAFTIR spectra increase with sonication time, suggesting electronic structural changes near the Fermi level. While their cause is presently unknown, it cannot be due to π-plasmon absorption of the MWCNTs,[27,28] since the slope increases with sonication time while both XPS and Raman spectroscopy indicate that no changes occur to the electronic structure during sonication.

We are led to the conclusion that aqueous sonication leads to the oxidation of $-CH_n$ groups already existing along the outer walls of the MWCNTs (the lack of structural damage found by our work indicates that the inner walls were inaccessible). Organic chemistry teaches that, in the absence of structural damage, primary C atoms (i.e., $-CH_3$) are capable of oxidizing to the primary $-$OH, then to $-C{=}O$ (aldehyde), and finally to $-$COOH. Secondary C atoms (i.e., $=CH_2$) are capable of oxidizing to the secondary $-$OH and, finally, to $-C{=}O$ (ketone). Tertiary C atoms (i.e., $\equiv$CH) can only oxidize to the tertiary $-$OH. Thus, the fact that $-$COOH was found in the O1s spectra (Figure 7) indicates the existence of $-$ CH_3 groups on the outer wall of the MWCNT. While some defects may be formed by chain scission, the experimental lack of further structural damage indicates that their concentration is too small to be of concern.

We interpret the initial surge of O2, in Figure 8, as the oxidation of $-CH_n$ to alcohol, which is reflected in the initial rapid overall oxidation rate in Figure 9a and that of O2 in Figure 9b. The decrease that follows this surge, in Figure 8, reflects the progressive oxidation of $-$OH to $-C{=}O$ and $-$COOH, under the mild energy input of the sonication process. The overall oxidation rate becomes slower, as seen in Figure 9a, as does that of O2 in Figure 9b. The roughly parallel slopes at extended periods of sonication, seen in Figure 9b, suggest that $-C{=}O$ and $-$ COOH production have similar rates, while the fact that O2 and O3 seem to reach a plateau, in Figure 8, suggests the initial presence of $=CH_2$ and perhaps $\equiv$CH as well as $-CH_3$; this supports our photoacoustic FTIR finding of multiple contributions to the $-CH_n$ vibrations at 2880$-$2990 cm^{-1}. Because of the present lack of understanding of the IR background, the relatively weak signals of the vibrational peaks, the low extent of oxidation (less than 3%, compared to acid sonication, which gives more than 6% plus structural damage[29,30]), and the overlap of O-containing and CNT skeletal peaks, more cannot be said at this time about the relative concentrations of $=CH_2$ and $\equiv$CH.

The production of O-containing groups appears to be the reason the increased ease of CNT dispersal in water occurs: these groups all participate in hydrogen bonding with water molecules. In a similar fashion, the $-$COOH groups, especially, lead to an increased interaction with the substrate, as seen in Figure 1: while hydrogen bonding occurs between adjacent CNTs, even stronger bonding occurs between $-$COOH groups and the Au substrate. The pK_a of Au surface hydroxide is near 3,[31] so that, at the pH of our aqueous system, near 7, the hydroxide has lost its proton and exists largely as $Au{-}O^-$; we have found that $-$ COOH forms strong hydrogen bonds to this group.[31] Similar results, presently being readied for publication, were found for silica substrates, which have a pK_a near 5. That is, the $-$COOH groups formed on the CNTs during sonication will preferentially hydrogen bond to the surface $Au{-}O^-$ groups, while hydrogen bonds between CNTs will occur mainly between $-$OH and $-$OH, or $-$OH and $-C{=}O$, both notably weaker.[31] The fact that all the CNTs lie horizontally in Figure 2 indicates that the oxidized $-$COOH groups that hydrogen bond to the

Au substrate are distributed along the lengths of the CNTs rather than at their ends.

Thus, the aqueous sonication of MWCNTs offers a pathway for improving the dispersal of CNTs in water; it is less physically damaging, and less contaminating, than sonication in acids or surfactants. The resultant increased CNTs interaction with the Au substrate, without mechanical (and, presumably, electronic) damage, also suggests that aqueous sonication has potential application as a tool for adhering individual CNTs on surfaces for microelectronics applications.

Conlusions

The aqueous sonication treatment of MWCNTs evinced no observable physical damage to the CNTs, improved aqueous dispersal and enhanced interaction with Au substrates. Spectroscopic analysis showed this to be due to the oxidation of $-CH_3$ groups to $-COOH$, which hydrogen bond strongly with both the aqueous medium and the $Au-O^-$ groups of the substrate. The increased stability of CNT dispersions, on sonication, is due to hydrogen bonding between the CNTs and the aqueous medium.

Acknowledgment. We thank the Natural Sciences and Engineering Research Council of Canada for funding, John H. T. Luong (Biotechnology Research Institute) for the gift of the MWCNTs, Souleymane Bah (École Polytechnique) for substrate preparations, and Alessandra M. Serventi (Institut National de Recherche Scientifique-Énergie, Matériaux et Télécommunications) for the HRTEM photomicrographs.

Supporting Information Available: Experimental data and photomicrographs supporting the assertion that no amorphous contaminant is produced, even after extensive sonication. This material is available free of charge via the Internet at http://pubs.acs.org.

References and Notes

(1) Shaffer, M. S. P.; Fan, X.; Windle, A. H. *Carbon* **1998**, *36*, 1603.
(2) Chen, J.; Hamon, M. A.; Hu, H.; Chen, Y. S.; Rao, A. M.; Eklund, P. C.; Haddon, R. C. *Science* **1998**, *282*, 95.
(3) Chen, J.; Rao, A. M.; Lyuksyutov, S.; Itkis, M. E.; Hamon, M. A.; Hu, H.; Cohn, R. W.; Eklund, P. C.; Colbert, D. T.; Smalley, R. E.; Haddon, R. C. *J. Phys. Chem.* **2001**, *B105*, 2525.
(4) Liu, L.-Q.; Zhang, S.-A.; Hu, T.-J.; Guo, Z.-X.; Ye, C.; Dai, L.-M.; Zhu, D.-B. *Chem. Phys. Lett*. **2002**, *359*, 191.
(5) Niyogi, S.; Hamon, M. A.; Perea, D. E.; Kang, C. B.; Zhao, B.; Pal, S. K.; Wyant, A. E.; Itkis, M. E.; Haddon, R. C. *J. Phys. Chem. B* **2003**, *107*, 8799.
(6) Liu, L.-Q.; Qin, Y.-J.; Guo, Z.-X.; Zhu, D.-B. *Carbon* **2003**, *41*, 331.
(7) Tasis, D.; Tagmatarchis, N.; Georgakilas, V.; Prato, M. *Eur.−Chem. J.* **2003**, *9*, 4000.
(8) Liu, Y.; Taylor, S.; Li, H.-P.; Fernando, K. A. S.; Qu, L.-W.; Wang, W.; Gu, L.-R.; Zhou, B.; Sun, Y.-P. *J. Mater. Chem*. **2003**, *14*, 527.
(9) Liu, J.; Rinzler, A. G.; Dai, H.; Hafner, J. H.; Bradley, R. K.; Boul, P. J.; Lu, A.; Iverson, T.; Shelimov, K.; Huffman, C. B.; Rodriguez-Macias, F.; Shon, Y. S.; Lee, T. R.; Colbert, D. T.; Smalley, R. E. *Science* **1998**, *280*, 1253.
(10) Islam, M. F.; Rojas, E.; Bergey, D. M.; Johnson, A. T.; Yodh, A. G. *Nano Lett*. **2003**, *3*, 269.
(11) Moore, V. C.; Strano, M. S.; Haroz, E. H.; Hauge, R. H.; Smalley, R. E. *Nano Lett*. **2003**, *3*, 1379.
(12) Lu, K.-L.; Lago, P. M.; Chen, Y. K.; Green, M. L. H.; Harris, P. J. F.; Tsang, S. C. *Carbon* **1996**, *34*, 814.
(13) Mukhopadhyay, K.; Dwivedi, C. D.; Mathur, G. N. *Carbon* **2002**, *40*, 1369.
(14) Luong, J. H. T.; Hrapovic, S.; Liu, Y.; Yang, D.-Q.; Sacher, E.; Wang, D.; Kingston, C. T.; Enright, G. D. *J. Phys. Chem. B* **2005**, *109*, 1400.
(15) Luong, J. H. T., private communication.
(16) Zhu, Y.-J.; Schnieders, A.; Alexander, J. P.; Beebe, T. P., Jr. *Langmuir* **2002**, *18*, 5728.
(17) Zielke, U.; Hüttinger, K. J.; Hoffman, W. P. *Carbon* **1996**, *34*, 983.
(18) Yang, D.-Q.; Sacher, E. *Surf. Sci*. **2002**, *504*, 125.
(19) Li, W.; Zhang, H.; Wang, C.; Zhang, Y.; Xu, L.; Zhu, K.; Xie, S. S. *Appl. Phys. Lett*. **1997**, *70*, 2684.
(20) Kastner, J.; Pichler, T.; Kuzmany, H. *Chem. Phys. Lett*. **1994**, *221*, 53.
(21) Kuhalmann, U.; Jantoljak, H.; Pfänder, N.; Bernier, P.; Journet, C.; Thomsen, C. *Chem. Phys. Lett.* **1998**, *294*, 237.
(22) Hamon, M. A.; Hu, H.; Bhowmik, P.; Niyogi, S.; Zhao, B.; Itkis, M. E.; Haddon, R. C. *Chem. Phys. Lett.* **2001**, *347*, 8.
(23) Branca, C.; Fusteri, F.; Magazú, V.; Mangione, A. *J. Phys. Chem. B* **2004**, *108*, 3469.
(24) Kuznetsova, A.; Mawhinney, D. B.; Naumenko, V.; Yates, J. T., Jr.; Liu, J.; Smalley, R. E. *Chem. Phys. Lett*. **2000**, *321*, 292.
(25) Bellamy, L. J. *The Infrared Spectra of Complex Molecules*, 2nd ed.; Methuen: London, 1959.
(26) Hiura, H.; Ebbesen, T. W.; Tanigaki, K.; Takahashi, H. *Carbon* **2001**, *39*, 569.
(27) Itkis, M. E.; Niyogi, S.; Meng, M. E.; Hamon, M. A.; Hu, H.; Haddon, R. C. *Nano Lett*. **2002**, *2*, 155.
(28) Haddon, R. C.; Sippel, J.; Rinzler, A. G.; Papadimitrakopoulos, F. *MRS Bull*. **2004**, *29*, 252.
(29) Liu, J.; Smalley, R. E. *Chem. Phys. Lett.* **2000**, *324*, 213.
(30) Ago, H.; Kugler, T.; Cacialli, F.; Salaneck, W. R.; Shaffer, M. S. P.; Windle, A. H.; Friend, R. H. *J. Phys. Chem. B* **1999**, *103*, 8116.
(31) Sylvestre, J.-P.; Kabashin, A.; Sacher, E.; Meunier, M.; Luong, J. H. T. *J. Am. Chem. Soc*. **2004**, *126*, 7176 and references therein. Sylvestre, J.-P.; Poulin, S.; Kabashin, A. V.; Sacher, E.; Meunier, M.; Luong, J. H. T. *J. Phys. Chem. B* **2004**, *108*, 16864.